Engineering Failure Analysis 161 (2024) 108223

Contents lists available at ScienceDirect

Engineering Failure Analysis

journal homepage: www.elsevier.com/locate/engfailanal

Effect of process parameters and film stratification on morphology and performance of auto-lubricating Ni-GnP electroplated coated steel

Gabriele Baiocco [a,*], Erica Menna [a], Emanuele Mingione [b], Gianluca Rubino [b], Nadia Ucciardello [a]

[a] *Dipartimento di Ingegneria dell'Impresa "Mario Lucertini", University of Rome of Tor Vergata, Via del Politecnico 1, 00133 Rome, Italy*
[b] *Università della Tuscia, DEIM, Largo dell'Università, 01100 Viterbo, Italy*

A R T I C L E I N F O

Keywords:
Industrial engineering
Coating
Nickel-Graphene
Electroplating
Co-deposition, wear, friction, lubrication

A B S T R A C T

Metal-matrix composites are of increasing interest in various industrial fields. The graphene reinforcement phase within the metal matrix structures makes it possible to enhance their properties and, thus, their performance in many contexts of use. Nickel is one of the most widely used materials to create such composites due to its mechanical and anti-corrosive qualities.

In particular, many nickel and graphene coatings are produced by electrodeposition. Despite being an extremely mature process, the production of composite coatings is not trivial, as the morphology of the film and the graphene inclusion and distribution within the bulk depends on different process parameters. The work aims to produce a self-lubricating composite coating of nickel and graphene nanoplatelets. Based on an initial implemented process, the layering of the layers coated and the mechanical agitation of the bath were varied to improve the inclusion of graphene in the matrix. The results showed that coating morphology is strongly affected by the process; also, an increment of film roughness and homogeneity does not necessarily translate into an increase in performance.

1. Introduction

Composite electrochemical coatings (CECs) are increasingly applied in many practical and research fields [1–3] to improve surface properties. Specifically, Nickel is one of the most widely used metals for diluting reinforcement [4]. Graphene nanosheets (GnS) and nanoplatelets (GnP) have been applied for Ni composite coatings production. Single-layer Graphene is a mono-atomic planar Carbon thin film [5,6] with outstanding physical and mechanical properties [7]. However, GnP presents easier production, storage and management and, despite containing more planar layers', it shows similar properties to single-layer materials, making this material the ideal reinforcement [8]. Many studies have proved how it can be effectively used as Ni matrix reinforcement to improve surface properties. Szeptycka et al. [9] achieved a composite Ni-Gr coating that increased the Ni wear and abrasion resistance, while Chen et al. [10] developed a Ni-Gr coating to increase hardness on steel substrates. In general, those coatings outperform the tribological performance of the CECs produced through other fillers such as chromium, boron nitride, zirconium dioxide, and PTFE [11]. Therefore, it has been extensively applied as a solid lubricant [12–15] and nanomaterial additive for composite films [16–21]. Indeed,

* Corresponding author.
E-mail address: gabriele.baiocco@uniroma2.it (G. Baiocco).

https://doi.org/10.1016/j.engfailanal.2024.108223
Received 21 November 2023; Received in revised form 13 February 2024; Accepted 11 March 2024
Available online 28 March 2024
1350-6307/

friction diminishes by interposing lubricant agents at the interfaces between two sliding parts, and lubricating coatings are already applied in many industrial fields nowadays [22–26]. Two principal types of metal composite have been proposed in the literature to enhance tribological performance. The composite film can be produced by dispersing graphene evenly within the metal [27–31] or by alternating metal layers with graphene layers to form a layered structure [32–34]. In any case, the combined structure aims to improve the mechanical properties according to mixed composition rules by preventing the dislocation from sliding within the lattice structure due to the Graphene flake embedded [8]. Among the different methods for producing composite coatings, electrodeposition is one of the most widely exploited electrochemical methods [35,36]. Indeed, electroplating is a cheap and stable process, extensively applied in industries as it is very mature, especially concerning Ni [37–40]. Also, it has already been applied successfully to produce a low-friction copper-graphene composite coating with a low friction coefficient and interesting lubricant properties [41]. Many studies have been presented to investigate how electroplating parameters affect coating properties such as thickness, morphology and mechanical performance as they change consistently with the process management [42–44]; additionally, these features also affect the graphene inclusion and distribution within the Ni matrix affecting the tribological performance [45]. The work aim, therefore, at producing a Nickel and GnP coating capable of exerting a lubricating action and ensuring a low coefficient of friction, implementing a deposition process for the production of a composite coating. Based on the first coatings and experimental tests, two strategies were developed to increase the inclusion of graphene in the matrix, the morphology of the layer and its performance. In particular, the stirring rate was considered along with the film layering by creating a layered structure with the addition of a final pure nickel coating. The results showed that the coating morphological characteristics can be improved, as well as the inclusion of graphene in the metal matrix. However, such improvements are not strictly correlated with an increase in performance.

2. Materials and methods

2.1. Materials

Nickel and Nickel-graphene depositions were performed on 3x4 cm^2 samples of DC01 steel, which composition is shown in Table 1.

The deposition process involves preliminary surface preparation by electrolytic degreasing and pickling; the processes were performed wet, using a commercial solution (Condoroine 155 and Descalinox 744P, purchased by Condoroil Chemical S.r.l.). The composite coating deposition were carried out through a cathodic deposition. The galvanic bath chosen for deposition is Watt's bath, based on nickel sulphate, nickel chloride and boric acid; the composition of the Nickel and Nickel-graphene deposition baths is briefly shown in Table 2.

The graphene used for the process was purchased by Nanesa and was in the form of graphene nanoplatelets (GnP), whose characteristics are summarized in Table 3; it is worth noting that the lateral dimensions of the reinforcement are high, with values as high as 100 μm, although the thickness is only a few atomic planes. As expressed by the D50 value, only 50% of the particles are below an average diameter of 42 μm.

2.2. Methods

2.2.1. Electroplating process

Ahead of the electrodeposition process, the surface of the DC01 samples was prepared by electrolytic degreasing and pickling. The former was performed cathodically with a stainless steel electrode inside a degreasing solution of distilled water and Condoroine 155 $8\%_{wt}$ (Condoroil Chemical S.r.l.) applying a voltage of 8 V for 3 min; the latter, by immersing the sample for 120 s in Descalinox 744P (Condoroil Chemical S.r.l.) solution in distilled water $10\%_{wt}$. Both processes were followed by rinsing in distilled water. The composite coating deposition were carried out through a cathodic deposition process with a laboratory set-up inside a 500 ml cylindrical becher, in which Nickel electrodes (anode) and the deposition substrate (cathode) were housed. The galvanic solution used was mechanically stirred. The process involves different phases; the first step involves a 5 μm layer coating of pure nickel, followed by 10 μm nickel-graphene composite coating deposition. However, according to preliminary results, action was necessary to improve the inclusion of graphene on the surface. For this purpose, two strategies were adopted: increasing the mechanical agitation of the bath (GnP/Ni_s) or the deposition of a final Nickel layer (GnP/Ni_Ni), as schematically shown in Fig. 1.

The coatings were compared with the non-deposited substrate and a pure Nickel deposit of 15 μm thickness. The duration of the galvanic process was determined as a function of the current density supplied to the system, according to Faraday's law. However, in the case of composite coatings, the thickness may differ considerably from the theoretical value due to different process efficiency and coating porosity. The process parameters used to produce the coatings are summarized in Table 4.

Table 1
DC01 steel composition.

	Element										
	Fe	C	P	Mn	Ni	Cr	S	Si	Mo	Cu	Al
Weight [%wt]	99.12	0.12	0.045	0.6	–	–	0.045	–	–	–	–

Table 2
Galvanic bath composition for each layer produced.

		Bath components				
		Nickel Sulphate [g/l]	*Nickel Chloride [g/l]*	*Boric Acid [g/l]*	*Sodium dodecyl sulfate [g/l]*	*GnP*
Layer	*Ni*	225	30	30	0	0
	Ni/GnP	225	30	–	0.1	1

Table 3
GnP technical datasheet 2022.

Property	Value	Unit
Appearance	powder	–
Carbon content	> 97	wt.%
C:O ratio	49:1	
Bulk density	0.07	g/cm^3
Specific surface area	56	m^2/g
Average flake thickness	8	nm
Layers	17	–
Average particles size (lateral)		
D90	96	µm
D50	42	µm

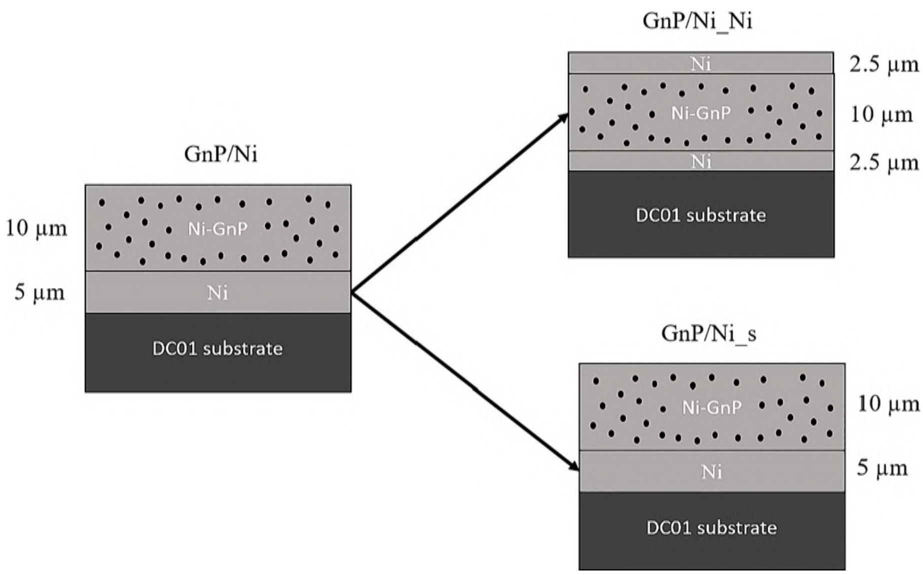

Fig. 1. Schematization of the composite coating produced.

Table 4
electroplating parameters exploited for the production of the composite coatings.

			Parameter		
			I [A/dm2]	*T [°C]*	*Stirring rate [rpm]*
Sample	*GnP/Ni*	Ni	3	20	250
		Ni-GnP	0.3	45	250
	GnP/Ni_s	Ni	3	20	250
		Ni-GnP	0.3	50	1000
	GnP/Ni_Ni	Ni	3	20	250
		Ni-GnP	0.3	50	250
		Ni	3	20	250

2.2.2. Morphological analysis

The sample analysis included the analysis of the surface by profilometry, which allowed the profile acquisition to evaluate the main roughness parameters and the reconstruction of surfaces' 3D maps; for the former, 30 profiles of 12.5 mm spaced 100 μm with a resolution of 1 μm were acquired while the latter required a 3x3mm^2 analysis with a spacing and resolution of 2 μm to create the maps. The roughness parameters evaluated are described as follows, while the respective equations are given in [46]:

- R_a, defined as the average absolute deviation of the roughness irregularities from the mean line over the sampling length;
- R_z, defined as the difference in height between the average of the five highest peaks and the five lowest valleys along the assessment length of the profile;
- R_{sm}, which represents the mean for the length of profile elements within the sampling length;
- $R_{\Delta q}$, which indicates the root mean square of the local tilt dZ/dX along the sampling length;
- R_{sk}, which is the third central moment of the profile amplitude probability density function, and measured over the assessment length;
- R_{ku}, which is the fourth central moment of the profile amplitude probability density function, measured over the assessment length

Also, SEM images were acquired to analyze the coating surface and structures.

2.2.3. Coating mechanical performance

Progressive scratch tests, ruled by the ASTM G171-03 standards, were also performed with a Rockwell diamond tip with a radius of 200 μm; the scratch length was equal to 3 mm with a load increasing linearly up to 30 N with a scratch speed of 1 mm/min. Dry sliding wear tests were performed to assess the friction coefficient through a 6 mm diameter alumina ball as a counterpart; the sliding velocity was equal to 5 cm/s, and the load was 1 N.

The test lasts up to a distance of 60 m. Finally, SEM images were acquired to highlight the morphology of the coating and wear trails. SEM-EDS analyses were also performed on the scratch trails to investigate the coating adhesion.

3. Results

3.1. Surface morphological assessment

Fig. 2 shows the 3D maps produced by profilometry for the scenarios investigated.

The nickel layer has a homogeneous morphology with a smooth surface similar to the untreated substrate, as evidenced by the St parameter on the map side (14.2 and 18.2, respectively); this value stands at 119.2 for the deposition of GnP within the metal matrix obtained with low mechanical stirring, which presents uniformly distributed peaks resulting from the graphene deposition; the flakes incorporate within the nickel matrix while the Ni ions reduce onto the substrate.

This mechanism anchors the GnP particles to the surface; however, the large dimension of the graphene flake produces a height displacement to the flat surface below; additionally, charge accumulation on graphene particles due to their higher conductivity alters the nucleation of Ni grains onto the surface, exacerbating the Nickel growth on preferential sites. Other works achieved Nickel-Graphene composites in which the friction experiencing an increase in roughness was found with the addition of reinforcement

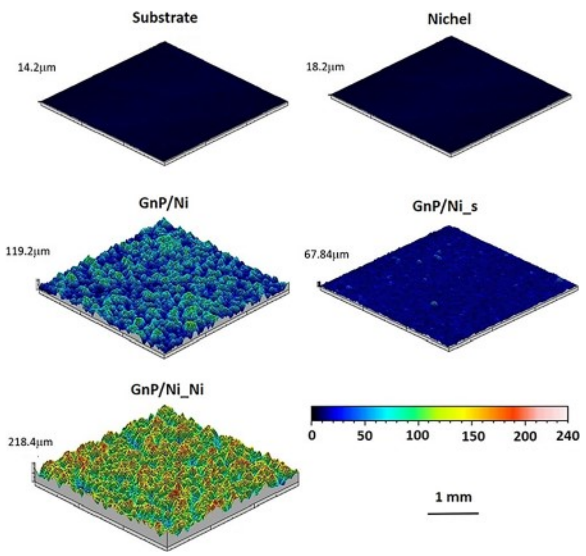

Fig. 2. 3D morphological representation of the coated samples.

[47,48] up to the creation of large clusters [49,50] of graphene on the surface; however, the extent of roughness is strongly dependent on the type of reinforcement used.

On the other hand, increasing the stirring rate results in a St reduction; the increased centrifugal force inside the deposition tank may push the higher mass and size flake away from the surface; therefore, the height displacement to the flat surface is flattened; also, the Nickel nucleation is more uniform along the whole surface, and the coating is homogeneous with a reduced St value, as highlighted by the 3D maps.

The Nickel deposition following the GnP/Ni coating is responsible for a severe increase of the St value over 200 μm; due to the high charge accumulation on the surface peaks, Ni ions reduce preferentially onto them, accentuating the Ni/GnP film morphology.

Fig. 3, which shows a profile for each scenario as an example, confirms this behavior.

The picture highlights the similarity between bare substrate and pure nickel profiles, as the pure Nickel resumes the substrate profile without altering its geometrical features; the GnP/Ni coating profile shows high peaks reaching over 50 μm height, which are equally distributed and alternate with a few tenths of a millimeter planar sections; in contrast, the increased stirring rate produces a higher number of surface peak characterized by reduced size and spacing confirming the presence of an increased number of nucleation site on the surface.

The pure Ni layer plated on the GnP/Ni replicates the underlying coating surface; the Ni ions reduction occurs at the surface asperities, increasing its height and width.

However, the increased peak cross-section decreases the space between two consecutive ridges; as a result, narrower and deeper valleys are visible.

The roughness parameters in Fig. 4 obtained from the surface analysis confirm what the qualitative morphological investigation suggested.

As expected, the DC01 substrate shows the lowest roughness parameters since being produced through a rolling process; however, pure Ni deposition does not substantially afflict the surface morphology and negligibly increases the roughness parameters.

On the other hand, the introduction of graphene deeply affects the surface morphology, increasing the roughness parameters measured.

The GnP/Ni and GnP/Ni_Ni samples exhibit the highest Ra and Rz values; the latter, which presents a nickel layer on top, shows slightly higher values.

On the other hand, the sample produced with a high stirring rate displays significantly lower values; a high roughness has already been associated with the filler presence inside a metal matrix, forming preferential nucleation zones [31]; however, it seems that the increased mechanical agitation of GnP/Ni_s forces the larger particles to move away from the electric double layer and thus reduces the size of the embedded reinforcement.

Also, it is worth noting that the spacing value (Rsm) obtained for this sample is also the smallest of all the scenarios; as the size of GnP on the surface reduces, the probability of lying between consecutive peaks increases, contributing to a decrease in the Rsm parameter's value.

Conversely, GnP/Ni and GnP/Ni_Ni have higher and similar values; this parameter considers homologous points on the profile, and the two scenarios have the same composite layer.

However, the latter has profiles with higher slopes compared to GnP/Ni because Ni deposition occurs preferentially on the asperities of the surface ridges, creating a non-constant coating thickness along its flank; in any case, the nickel end-coverage improves the reinforcement covering and coating continuity.

The GnP/Ni and GnP/Ni_s composite films have positive Rsk values, as opposed to GnP/Ni_Ni; this value indicates that, despite deposition occurring preferentially on the clusters, the increase in their size goes so far as to fill the existing gap, reproducing and

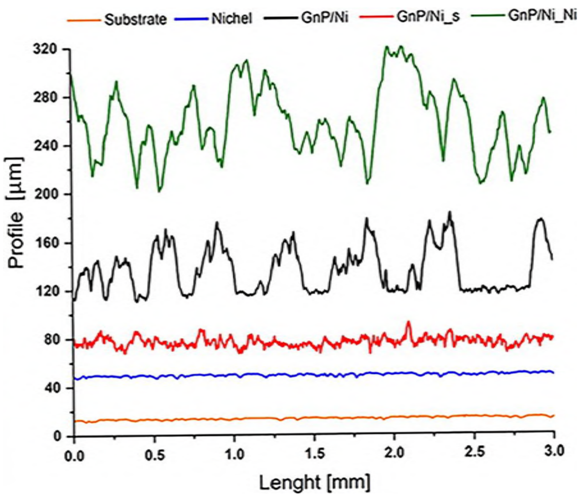

Fig. 3. Surface profiles derived from 3d maps.

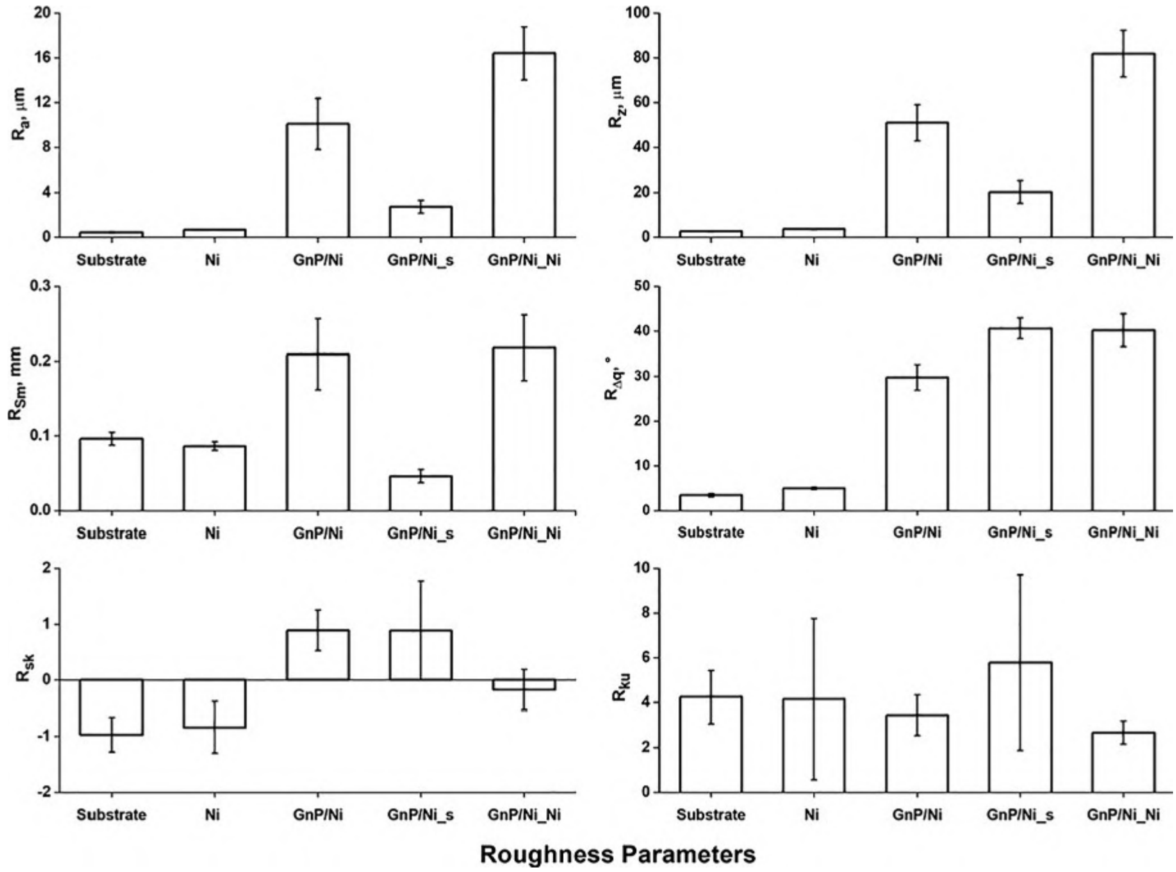

Fig. 4. roughness parameters measured on deposited surfaces.

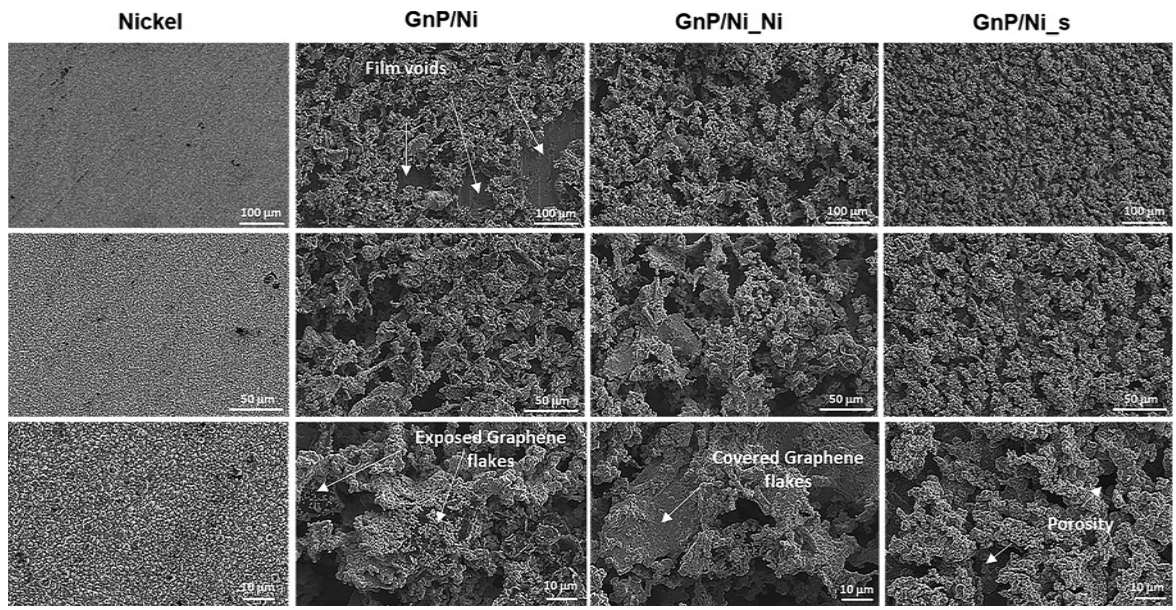

Fig. 5. SEM images at different magnifications of the composite coatings obtained.

exasperating the underlying morphology but creating a profile with a predominance of peaks and narrow valleys, albeit very deep.

The SEM images in Fig. 5 highlight these morphologies.

As expected, the Ni coating has a compact and homogenous structure; even at higher magnifications, the lack of discontinuities and surface defects is evident, as well as a homogenous nucleation of the metal on the surface; in contrast, the graphene introduction significantly modifies the coating morphology, which shows a highly uneven and non-homogeneous surface.

The presence of columnar structures characterizes these three scenarios, with irregular shapes that rise from the surface interspersed with planar areas where the film is not deposited; these structures, due to the shape irregularity, create a coating with high porosity.

However, the extent of these features is highly dependent on the process implemented, as shown in the low-magnification SEM images; while the film voids are evident in the GnP/Ni sample, which exhibits large uncoated areas, they are no longer present as far as GnP/Ni_Ni and GnP/Ni_s samples are concerned; in addition, the latter display a uniform coating with small adjacent cluster whereas the former highlights more spaced columnar structures like in GnP/Ni.

Nonetheless, higher magnifications show that the composite coating structure remains mostly unaffected and characterized by columnar structures, although in GnP/Ni_s the scale of their dimension is lower.

The dense GnP/Ni_s structure, although showing small surface clusters, leads to a porous layer that includes the graphene thoroughly; the increased agitation prevents the large particles from being deposited as the centrifugal force pushes them apart from the sample surface.

As visible at higher magnifications, in GnP/Ni the graphene is not fully included within the metal structure; although anchored to the sample surface by the Ni ions' reduction, the GnP flakes in the surface clusters are not covered thoroughly.

The Nickel covering the GnP/Ni_Ni sample allows the filling of the planar spaces between the columnar structures, completing the inclusion of the reinforcement within the matrix and creating a more homogeneous coating on the substrate. In addition, the Nickel deposited in GnP-functionalized substrates has a higher nucleation during the electrodeposition process, which results in the forming of an increased number of grains along with a general reduction in their size, as shown in Fig. 6, despite this does not lead to the development of a consistent layer for the reasons discussed above.

Fig. 7 shows the EDS investigations performed on the GnP/Ni sample in distinct areas of its surface; in particular, the analysis was performed on the clusters (Fig. 7a) and the planar space (Fig. 7b).

The measured spectra display a clear difference in composition; the latter shows significantly higher percentages of carbon and oxygen than the investigated planar space, whose composition is predominantly Nickel.

This difference suggests that the coating obtained is not actually continuous, but the graphene deposit on the surface above which the deposition of Nickel occurs embedding the graphene flake; as the reduction of Ni ions continues, the clusters enlarge, touching each other to create a coating characterized by high porosity.

With a decrement in the size of the surface reinforcement, more preferential nucleation sites are present, leading to the formation of a more compact film.

3.2. *Mechanical performance evaluation: Scratch and wear test*

Fig. 8 shows the scratch curves obtained to assess the coating's adhesion to the substrate.

The chart highlights the similar trend that characterizes DC01 and Nickel in terms of Pd and Rd, with the lower values. Both show a linearly increasing trend with the applied load. Nickel, which has higher hardness than the substrate, shows slightly lower Pd values; both DC01 and Ni Rd curves, on the other hand, exhibit a sharp reduction at higher loads. Pure Nickel displays a higher Rd value

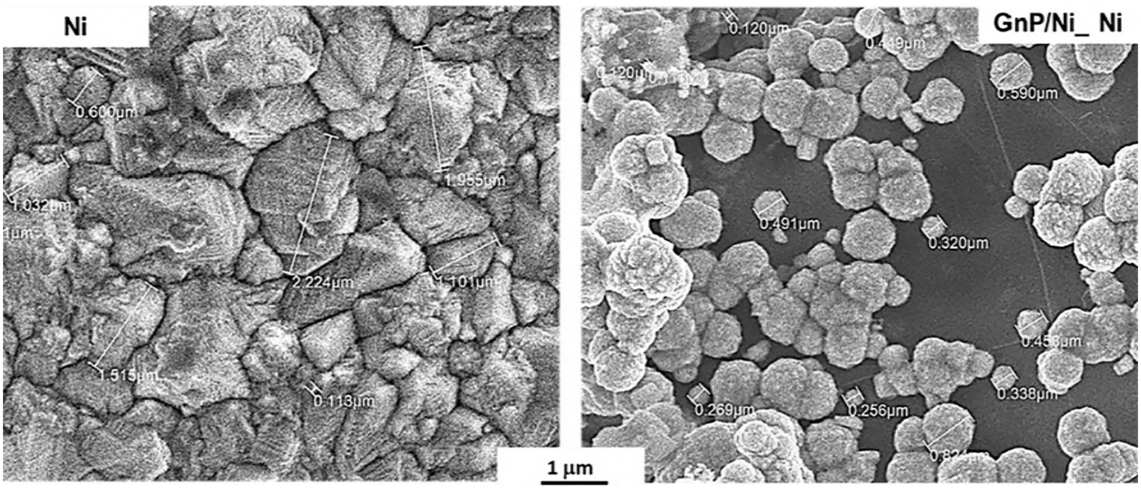

Fig. 6. SEM images at different magnifications of the composite coatings obtained.

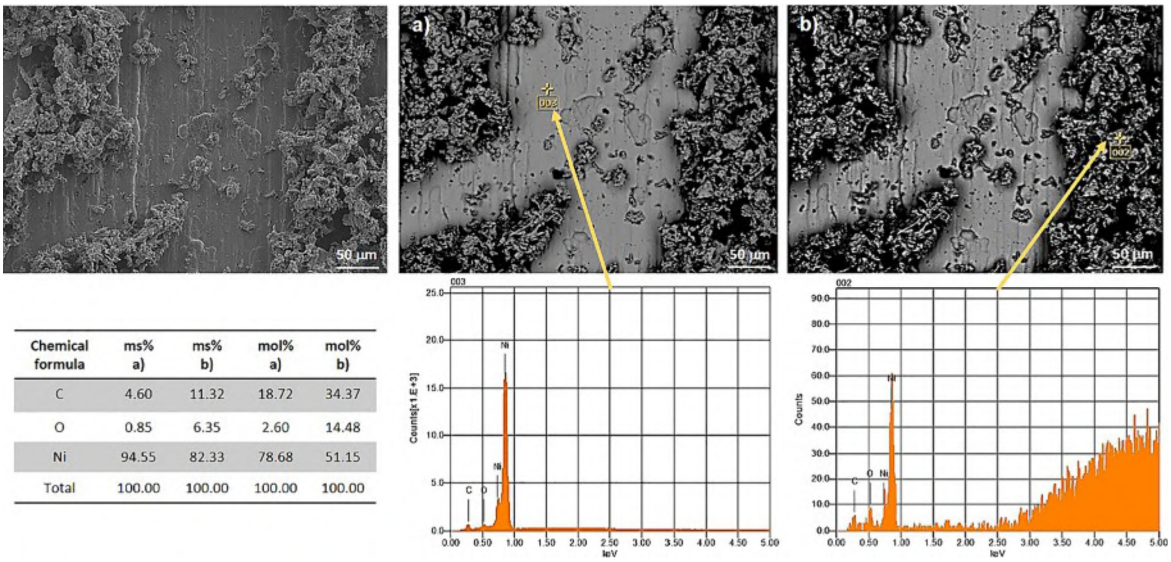

Chemical formula	ms% a)	ms% b)	mol% a)	mol% b)
C	4.60	11.32	18.72	34.37
O	0.85	6.35	2.60	14.48
Ni	94.55	82.33	78.68	51.15
Total	100.00	100.00	100.00	100.00

Fig. 7. EDS analysis of the GnP/Ni sample (a) in the planar zone between contiguous clusters and (b) within a cluster.

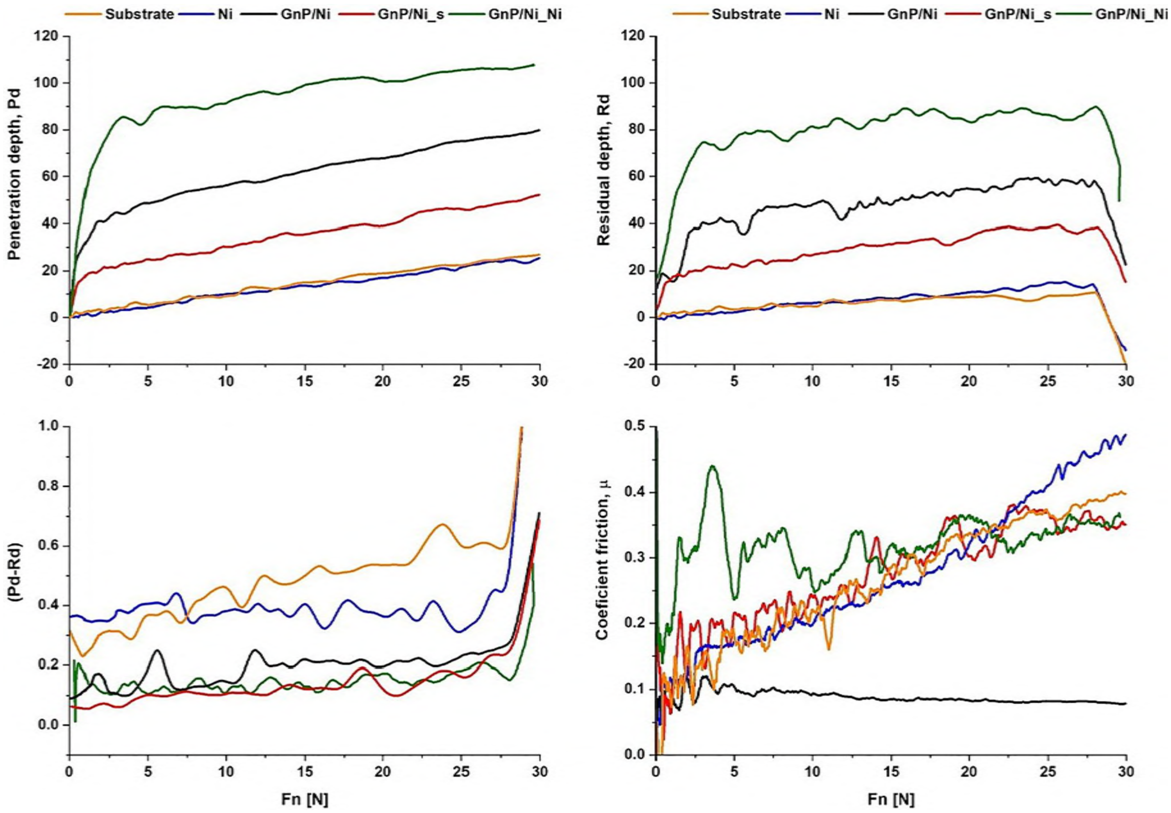

Fig. 8. Penetration and friction curves as a function of load obtained in the scratch test.

towards the end of the trace than the substrate; this behavior is caused by the coating compaction at the end of the track following the action of the indenter after 20 N. Also, it is worth noting that around 27 N, in both scenarios, the residual depth decreases sharply for both the Ni coating and the non-deposited substrate; the material in front of the indenter tip undergoes compressive stress, and if the film has good cohesion and adhesion to the substrate, it accumulates at the end of the scratch track, and the indenter detects the build-up material when measuring the residual depth, producing negative values of this parameter.

Conversely, the Pd and Rd values of composite coatings are significantly higher, and the curves show a steep initial section followed by a similar trend in Ni and DC01. The graphene inclusion increases the surface roughness, producing columnar and irregular structures that result in porous film. Therefore, the indenter encounters an initial phase where the coating feasibly penetrates; as it advances, it exerts compressive stress on the underlying layer and produces film compaction o. In general, a correspondence emerges between the values of Rz and maximum penetration; therefore, the smoother and more homogeneous the film with close surface ridges of reduced height, the lower the penetration depth. It appears that the indenter, during its run, homogeneously flattens the coating. This behavior is evident in the final segment of the Rd curves; flattening of the composite film, along with possible partial damage and coating delamination, results in a limited pile-up, with the Rd value remaining lower than zero at the end of the trace. This trend also seems to be confirmed by the Pd-Rd values, a springback index, which is lower for the composite coatings. However, it is worth noting that in all scenarios, GnP/Ni is the only one capable of exerting an effective lubricating action, as highlighted in the friction curves of Fig. 8. In general, the coefficient of friction increases with load as the indenter increases the contact area with the coating as it penetrates the surface, and the tangential force increases accordingly. However, in the case of GnP/Ni, the coefficient of friction is around 0.1, with a slightly decreasing trend with the applied load. Despite having a high Pd value, the action of the tip will probably dislodge the graphene lying between the indenter and the surface.

Fig. 9 shows the SEM images of the trace morphology. The pure nickel trace shows no delamination or coating breakage; as Fig. 9 highlights, the coating is subject to a micro ploughing mechanism and flows plastically to the sides of the indenter, creating a lateral pile-up, in addition to the one at the head of the wear track as deduced from the wear curves.

On the opposite, the GnP/Ni and GnP/Ni_Ni samples show clear signs of coating detachment at the scratch track sides; the conical shape of the indenter, as the test progresses, exerts shear stresses on the columnar structures adjacent to the track, which detach from the substrate as they are shear-stressed; in the former, however, the extent of the delamination is greater, affecting a broader coating portion; on the contrary, in the GnP/Ni_Ni sample the final metal covering seems to increase the coating cohesion, preventing the process from expanding outside the scratch trace; within the scratch trail, on the other hand, the compressive stresses are such as to compact the porous coating, which therefore does not accumulate at the end of the scratch trace but remains adherent to the surface, interposing itself between the tip and the substrate and exerting, in the case of the GnP/Ni sample, a lubricating action. The film compaction is particularly noticeable in GnP/Ni_s, which presents a homogeneous wear track with well-defined edges.

The images in Fig. 10 achieved by EDS analysis allow an in-depth analysis of the scratch trails. The EDS maps show that the Nickel coating does not suffer any damage, flowing plastically to the sides of the tip and suffering no delamination. In contrast, the GnP/Ni sample breaks up, producing a delamination of the coating that goes well beyond the edges of the trace, revealing the underlying Nickel substrate. The presence of prominent asperities on the surface accentuates the stress concentration factor, and the graphene particles subjected to shear tensions during the indenter's run do not retain their adhesion to the substrate. However, no Iron is detected in the spectrum, indicating that the coating remains adhered and does not expose the DC01 steel substrate; in contrast, the final Nickel coating reduces the delamination experienced by the film, which is instead compacted within the trace, as shown by the high Nickel concentrations detected. This compaction allows the graphene to stay inside the trail, in contrast to what happens in GnP/Ni; in the latter case, in fact, high amounts of GnP (Carbon) are not detected, which, under the action of the indenter, detach themselves from the coating. By interposing itself between the base Nickel and the indenter, it manages to exert a lubricating function, unlike the GnP/Ni_Ni scenario. In GnP/Ni_s, the presence of narrow asperities close to each other allows the formation of a film with greater compactness and consistency, preventing delamination without an additional nickel coating, with the film compacted as the tip travels. As with GnP/Ni_Ni, the graphene remains encapsulated within the track due to the compression of the coating, thus being unable to exert a lubricating action; furthermore, as the high stirring draws the heavier reinforcements away, the carbon signal is lower.

The wear tests, whose curves are shown in Fig. 11, confirm the above in relation to the friction coefficient. As expected, the substrate has the highest coefficient of friction, varying between 0.5 and 0.6 during the test. The specimen coated with Nickel, which has a higher hardness than the substrate, presents a significantly lower friction coefficient after an initial stretch when the contact between counterpart and sphere settles. The composite coatings show highly different behavior.

As highlighted in the literature, the test generates an oxide tribofilm which is broken producing debris [51]; due to the discontinuity a metal-to-metal contact is created, producing a slight adhesive wear, as well as triboxidative wear. The same mechanism was found in [47], where the presence of reinforcing particles within the oxide layer is highlighted, which, although discontinuous, are able to reduce friction and wear, also highlighting the formation of a carbon-rich lubricating surface layer.

The GnP/Ni sample shows the lowest coefficient of friction, with a stable and constant value of about 0.15 throughout the test. In spite of a high roughness, there is not a high resistance to advancing as the pin causes the clusters to break due to the high porosity. In the authors' opinion, the flakes breaking are interposed between the pin and the surface, avoiding the metal-to-metal contact and mitigating the tangential force required for motion, which is proportional to the friction coefficient measured, as shown in [47] and [48]; a slight increase in the friction coefficient is observed as the test continues, which may be due to the consumption of the graphene particles not anchored to the surface and the progressive widening of the track and thus of the contact surface with the counterpart. Nickel deposition, however, worsens the friction value, which is higher than Nickel and fluctuates during the duration of the test. The graphene remaining within the coating fails to act as an interface element and to balance the effect of the high roughness produced. During the experiment, just part of the included graphene was exposed and interposed between counterpart and surface, achieving partial and discontinuous lubrication over time.

Increased agitation reduces the size of the embedded reinforcements and, consequently, worsens the value of the friction coefficient. In the case of GnP/Ni_s, although a uniform distribution of the nanosheets should improve the behavior [50,52], the lower amount of graphene is not such as to allow the formation of a tribofilm [53]. Therefore, friction increases due the high surface

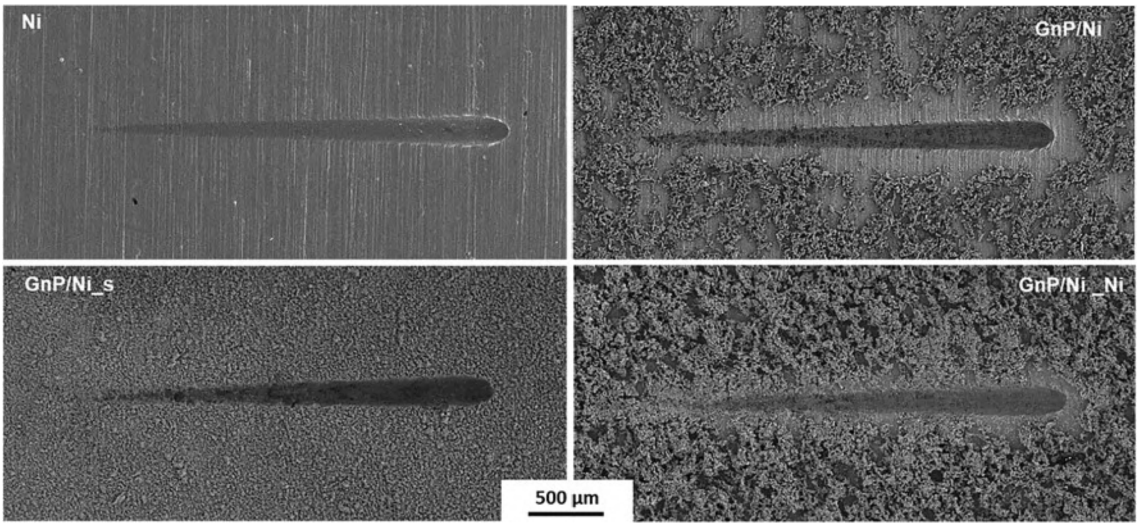

Fig. 9. SEM images of scratch marks on coatings.

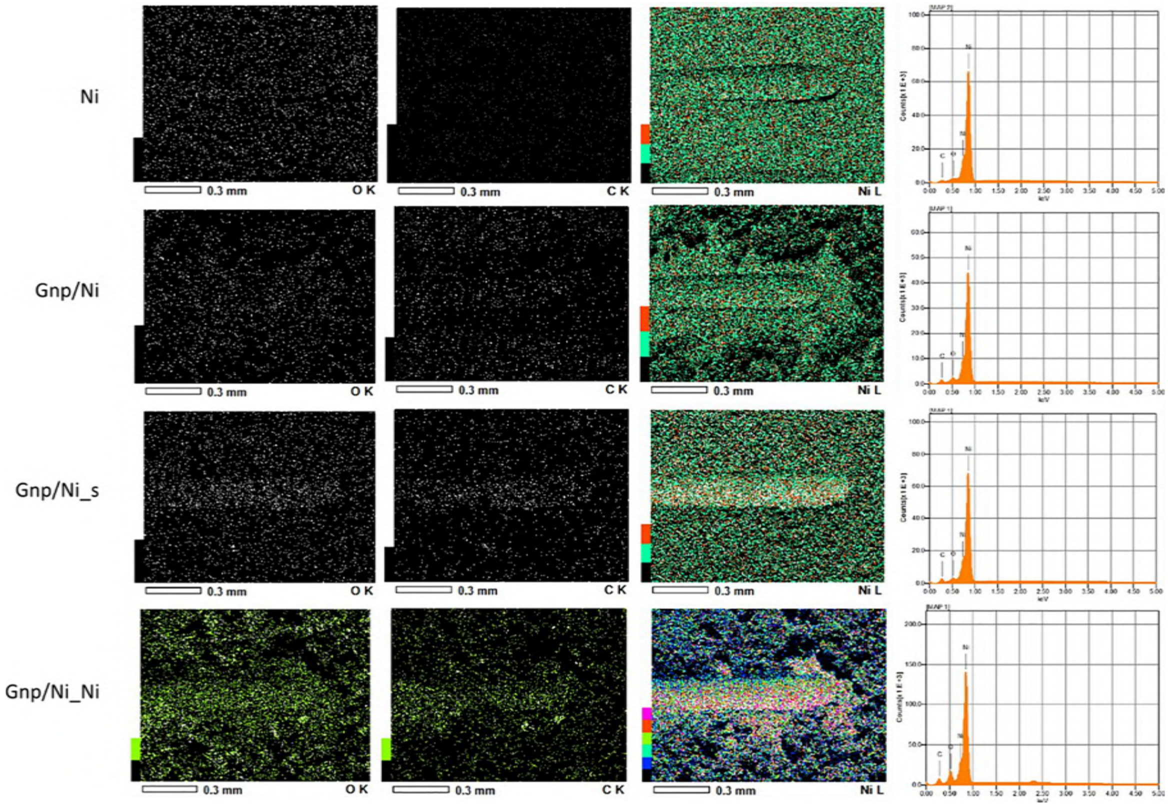

Fig. 10. EDS maps of the scratch trails.

roughness [53], which is higher than that of pure nickel. In any case, the homogenous and compact structure of the coating, which also has the lowest roughness, makes it possible to obtain a more constant course of this value over time.

Fig. 12 shows the SEM images of the worn trail. Of all the coatings, Nickel has the narrower wear trace; the hardness of the material, in addition to a smooth surface and the high film density, leads to reduced wear, maintaining the coating adhered to the substrate.

Conversely, the traces produced on GnP/Ni and GnP/Ni_Ni show traces of comparable size as the composite layers are similar. The trail of the former, however, seems to be slightly larger; as the coating is less compact, the sphere gradually penetrates, wearing it down but, at the same time, revealing the graphene inside that acts as a lubricant. The final Ni coating appears to reduce the wear of the film

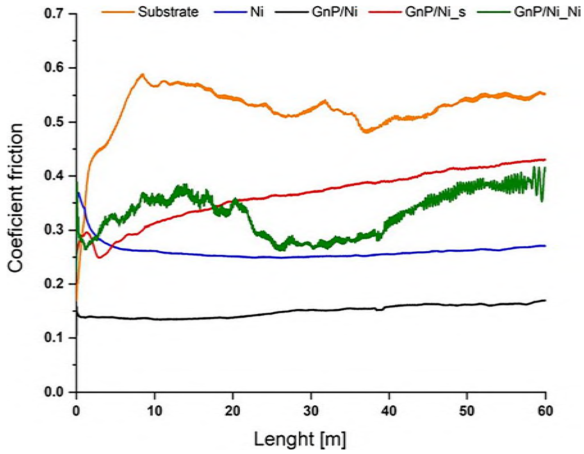

Fig. 11. Friction coefficient VS sliding distance.

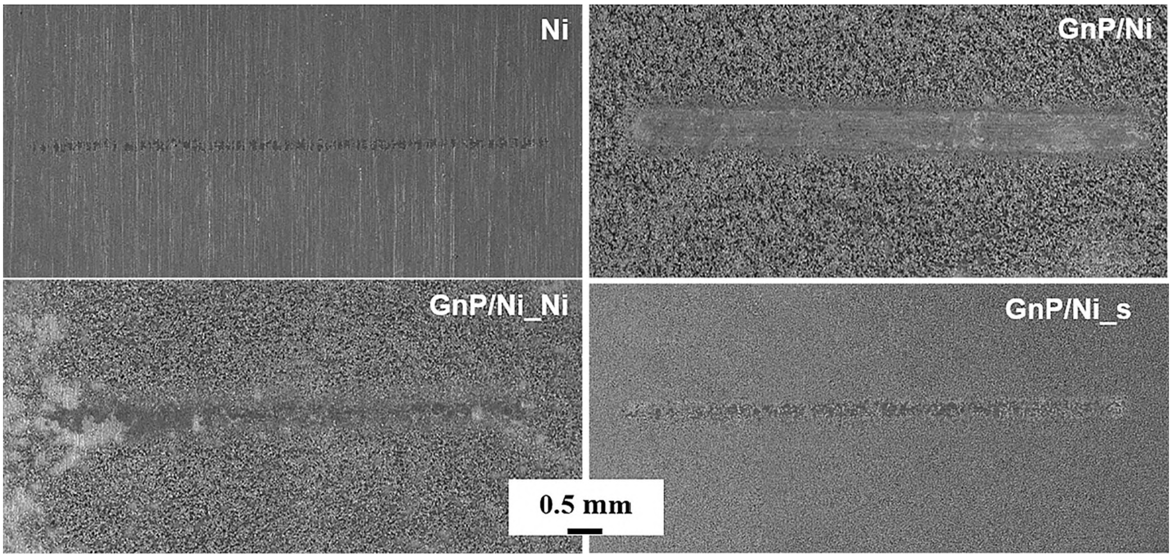

Fig. 12. SEM images of the trails obtained from the dry sliding test.

slightly, increasing its cohesion. However, this does not allow the trapped graphene to reach the surface, leaving it embedded at the bottom of the trace. On the other hand, the sample produced with the higher stirring has a wear trace of intermediate size. While the inclusion of graphene is not such to allow efficient lubrication, the film structure is such that it compacts under the action of the counterpart without suffering delamination or excessive damage, unlike the GnP/Ni sample.

4. Conclusion

This paper investigated the self-lubricating properties of a composite coating in which graphene is dispersed within a pure nickel matrix by electrodeposition. In particular, the work studied how different processing parameters impact the morphology and effectiveness of a nickel-graphene composite coating produced on a steel substrate. To this end, the layering and mechanical agitation of the bath were varied on the basis of preliminary Nickel-graphene coating. The main results achieved are listed as follow:

- Graphene acts as a preferential nucleation site for nickel during ion reduction, leading to a rough deposit with large GnP particles.
- The nickel-graphene composite coating is partly non-continuous, with GnP particles partially uncovered, and requires proper interposition for effective lubrication.
- Stirring in the bath helps create a more homogeneous film by pushing larger particles away, resulting in a coating where smaller flakes are more evenly distributed.

- The final nickel coating allows graphene to embed and enhances the underlying morphology, contributing to a more effective and consistent structure.
- Wear tests show that GnP/Ni composite achieves the lowest friction coefficient (0.15), forming a lubricant layer during the test. Other composite coatings perform worse than pure Ni.
- Large clusters in the coating lead to cracking under shear and compressive stresses, causing delamination and exposing the substrate.
- Films with higher stirring and nickel top coatings exhibit a more homogeneous and consistent structure, indicating the importance of optimizing processing parameters for enhanced structural integrity and lubricating properties.
- The study highlights the intricate relationship between processing parameters, coating morphology, and lubrication effectiveness in nickel-graphene composite coatings on steel substrates.

Funding

This research did not receive any specific grant from funding agencies in the public, commercial, or not-for-profit sectors.

CRediT authorship contribution statement

Gabriele Baiocco: Writing – review & editing, Writing – original draft, Investigation, Formal analysis. **Erica Menna:** Methodology, Investigation. **Emanuele Mingione:** Writing – review & editing, Writing – original draft, Investigation. **Gianluca Rubino:** Writing – original draft, Validation, Methodology, Formal analysis, Conceptualization. **Nadia Ucciardello:** Validation, Supervision, Resources, Conceptualization.

Declaration of competing interest

The authors declare that they have no known competing financial interests or personal relationships that could have appeared to influence the work reported in this paper.

Data availability

The data that has been used is confidential.

References

[1] A. Góral, L. Lityńska-Dobrzyńska, M. Kot, Effect of surface roughness and structure features on tribological properties of electrodeposited nanocrystalline Ni and Ni/Al2O3 coatings, J. Mater. Eng. Perform. 26 (2017) 2118–2128, https://doi.org/10.1007/s11665-017-2662-2.
[2] M.H. Allahyarzadeh, M. Aliofkhazraei, A.R. Rezvanian, V. Torabinejad, A.R. Sabour Rouhaghdam, Ni-W electrodeposited coatings: characterization, properties and applications, Surf. Coat. Technol. 307 (2016) 978–1010, https://doi.org/10.1016/j.surfcoat.2016.09.052.
[3] E. Ali, Solid lubricants and self-lubricating films, in: Modern Tribology Handbook, Two Volume Set, CRC Press, 2000. doi: 10.1201/9780849377877.
[4] A. Siddaiah, P. Kumar, A. Henderson, M. Misra, P.L. Menezes, surface energy and tribology of electrodeposited Ni and Ni–graphene coatings on steel, Lubricants. 7 (2019) 87, https://doi.org/10.3390/lubricants7100087.
[5] Y. Tang, X. Yang, R. Wang, M. Li, Enhancement of the mechanical properties of graphene–copper composites with graphene–nickel hybrids, Mater. Sci. Eng. A 599 (2014) 247–254, https://doi.org/10.1016/j.msea.2014.01.061.
[6] K.S. Novoselov, A.K. Geim, S.V. Morozov, D. Jiang, Y. Zhang, S.V. Dubonos, I.V. Grigorieva, A.A. Firsov, Electric field effect in atomically thin carbon films, Science 306 (2004) (1979) 666–669.
[7] L. Zhang, N. Li, H. Xia, J. Zhang, P. Zhang, M. Xu, H. Ma, Preparation and mechanical properties of (Ni-Fe)-graphene composite coating, Adv. Eng. Mater. 18 (2016) 1716–1719, https://doi.org/10.1002/adem.201600357.
[8] Z. Ren, N. Meng, K. Shehzad, Y. Xu, S. Qu, B. Yu, J.K. Luo, Mechanical properties of nickel-graphene composites synthesized by electrochemical deposition, Nanotechnology 26 (2015) 065706, https://doi.org/10.1088/0957-4484/26/6/065706.
[9] B. Szeptycka, A. Gajewska-Midzialek, Nickel-Graphene composite coatings, Compos. Theory Pract. 15 (2015) 107–111.
[10] J. Chen, J. Li, D. Xiong, Y. He, Y. Ji, Y. Qin, Preparation and tribological behavior of Ni-graphene composite coating under room temperature, Appl. Surf. Sci. 361 (2016) 49–56, https://doi.org/10.1016/j.apsusc.2015.11.094.
[11] C. Donnet, A. Erdemir, Historical developments and new trends in tribological and solid lubricant coatings, Surf. Coat. Technol. 180–181 (2004) 76–84, https://doi.org/10.1016/j.surfcoat.2003.10.022.
[12] E. Sadeghinezhad, M. Mehrali, R. Saidur, M. Mehrali, S. TahanLatibari, A.R. Akhiani, H.S.C. Metselaar, A comprehensive review on graphene nanofluids: recent research, development and applications, Energy Convers. Manag. 111 (2016) 466–487, https://doi.org/10.1016/j.enconman.2016.01.004.
[13] A.K. Rasheed, M. Khalid, W. Rashmi, T.C.S.M. Gupta, A. Chan, Graphene based nanofluids and nanolubricants – Review of recent developments, Renew. Sustain. Energy Rev. 63 (2016) 346–362, https://doi.org/10.1016/j.rser.2016.04.072.
[14] E.D. Ramón-Raygoza, C.I. Rivera-Solorio, E. Giménez-Torres, D. Maldonado-Cortés, E. Cardenas-Alemán, R. Cué-Sampedro, Development of nanolubricant based on impregnated multilayer graphene for automotive applications: analysis of tribological properties, Powder Technol. 302 (2016) 363–371, https://doi.org/10.1016/j.powtec.2016.08.072.
[15] D. Blanco, R. González, J.L. Viesca, A. Fernández-González, M. Bartolomé, A. Hernández Battez, Antifriction and antiwear properties of an ionic liquid with fluorine-containing anion used as lubricant additive, Tribol. Lett. 65 (2017) 66, https://doi.org/10.1007/s11249-017-0846-4.
[16] A. Dorri Moghadam, E. Omrani, P.L. Menezes, P.K. Rohatgi, Mechanical and tribological properties of self-lubricating metal matrix nanocomposites reinforced by carbon nanotubes (CNTs) and graphene – a review, Compos. B Eng. 77 (2015) 402–420, https://doi.org/10.1016/j.compositesb.2015.03.014.
[17] M. Tabandeh-Khorshid, E. Omrani, P.L. Menezes, P.K. Rohatgi, Tribological performance of self-lubricating aluminum matrix nanocomposites: role of graphene nanoplatelets, Eng. Sci. Technol. Int. J. 19 (2016) 463–469, https://doi.org/10.1016/j.jestch.2015.09.005.
[18] A.K. Kasar, G. Xiong, P.L. Menezes, Graphene-reinforced metal and polymer matrix composites, JOM 70 (2018) 829–836, https://doi.org/10.1007/s11837-018-2823-2.

[19] A.K. Kasar, P.L. Menezes, Synthesis and recent advances in tribological applications of graphene, Int. J. Adv. Manuf. Technol. 97 (2018) 3999–4019, https://doi.org/10.1007/s00170-018-2019-5.
[20] E. Omrani, P. Menezes, P. Rohatgi, Effect of micro- and nano-sized carbonous solid lubricants as oil additives in nanofluid on tribological properties, Lubricants. 7 (2019) 25, https://doi.org/10.3390/lubricants7030025.
[21] E. Omrani, P.K. Rohatgi, P.L. Menezes, Tribology and Applications of Self-Lubricating Materials, CRC Press, Boca Raton : CRC Press, Taylor & Francis, 2017, 2017. doi: 10.1201/9781315154077.
[22] M.-B.-K. Gabel, J.J. Bethke, Coatings for fretting prevention, Wear 46 (1978) 81–96, https://doi.org/10.1016/0043-1648(78)90112-6.
[23] T. Spalvins, Coatings for wear and lubrication, Thin Solid Films 53 (1978) 285–300, https://doi.org/10.1016/0040-6090(78)90222-5.
[24] M.H. Zhu, Z.R. Zhou, An investigation of molybdenum disulfide bonded solid lubricant coatings in fretting conditions, Surf. Coat. Technol. 141 (2001) 240–245, https://doi.org/10.1016/S0257-8972(01)01194-X.
[25] J.P.G. Farr, Molybdenum disulphide in lubrication. A review, Wear. 35 (1975) 1–22, https://doi.org/10.1016/0043-1648(75)90137-4.
[26] K. Friedrich, A.K. Schlarb, Tribology of Polymeric Nanocomposites: Friction and Wear of Bulk Materials and Coatings, Elsevier, Amsterdam, 2008.
[27] J. Hwang, T. Yoon, S.H. Jin, J. Lee, T.-S. Kim, S.H. Hong, S. Jeon, Enhanced mechanical properties of graphene/copper nanocomposites using a molecular-level mixing process, Adv. Mater. 25 (2013) 6724–6729, https://doi.org/10.1002/adma.201302495.
[28] Z. Li, G. Fan, Z. Tan, Q. Guo, D. Xiong, Y. Su, Z. Li, D. Zhang, Uniform dispersion of graphene oxide in aluminum powder by direct electrostatic adsorption for fabrication of graphene/aluminum composites, Nanotechnology 25 (2014) 325601, https://doi.org/10.1088/0957-4484/25/32/325601.
[29] L.-Y. Chen, H. Konishi, A. Fehrenbacher, C. Ma, J.-Q. Xu, H. Choi, H.-F. Xu, F.E. Pfefferkorn, X.-C. Li, Novel nanoprocessing route for bulk graphene nanoplatelets reinforced metal matrix nanocomposites, Scr. Mater. 67 (2012) 29–32, https://doi.org/10.1016/j.scriptamat.2012.03.013.
[30] J. Wang, Z. Li, G. Fan, H. Pan, Z. Chen, D. Zhang, Reinforcement with graphene nanosheets in aluminum matrix composites, Scr. Mater. 66 (2012) 594–597, https://doi.org/10.1016/j.scriptamat.2012.01.012.
[31] G. Baiocco, E. Menna, G. Rubino, N. Ucciardello, Mechanical characterization of functional Cu-GnP composite coatings for lubricant applications, Surf. Eng. 38 (2022) 72–78, https://doi.org/10.1080/02670844.2022.2040187.
[32] Y. Kim, J. Lee, M.S. Yeom, J.W. Shin, H. Kim, Y. Cui, J.W. Kysar, J. Hone, Y. Jung, S. Jeon, S.M. Han, Strengthening effect of single-atomic-layer graphene in metal–graphene nanolayered composites, Nat. Commun. 4 (2013) 2114, https://doi.org/10.1038/ncomms3114.
[33] J.S. Carpenter, A. Misra, P.M. Anderson, Achieving maximum hardness in semi-coherent multilayer thin films with unequal layer thickness, Acta Mater. 60 (2012) 2625–2636, https://doi.org/10.1016/j.actamat.2012.01.029.
[34] Y. Xu, W. Hong, H. Bai, C. Li, G. Shi, Strong and ductile poly(vinyl alcohol)/graphene oxide composite films with a layered structure, Carbon N Y. 47 (2009) 3538–3543, https://doi.org/10.1016/j.carbon.2009.08.022.
[35] C.T.J. Low, R.G.A. Wills, F.C. Walsh, Electrodeposition of composite coatings containing nanoparticles in a metal deposit, Surf. Coat. Technol. 201 (2006) 371–383, https://doi.org/10.1016/j.surfcoat.2005.11.123.
[36] B. Szeptycka, A. Gajewska-Midzialek, T. Babul, Electrodeposition and corrosion resistance of Ni-graphene composite coatings, J. Mater. Eng. Perform. 25 (2016) 3134–3138, https://doi.org/10.1007/s11665-016-2009-4.
[37] A. Ibáñez, R. Escudero-Cid, P. Ocón, E. Fatás, Effect of the pulse plating parameters on the mechanical properties of nickel electrodeposits, Surf. Coat. Technol. 212 (2012) 94–100, https://doi.org/10.1016/j.surfcoat.2012.09.027.
[38] J.K. Luo, M. Pritschow, A.J. Flewitt, S.M. Spearing, N.A. Fleck, W.I. Milne, Effects of process conditions on properties of electroplated Ni thin films for microsystem applications, J. Electrochem. Soc. 153 (2006) D155, https://doi.org/10.1149/1.2223302.
[39] W. Shao, D. Nabb, N. Renevier, I. Sherrington, Y. Fu, J. Luo, Mechanical and anti-corrosion properties of TiO_2 nanoparticle reinforced Ni coating by electrodeposition, J. Electrochem. Soc. 159 (2012) D671–D676, https://doi.org/10.1149/2.065211jes.
[40] C.K. Chung, W.T. Chang, Effect of pulse frequency on the morphology and nanoindentation property of electroplated nickel films, Microsyst. Technol. 13 (2007) 537–541, https://doi.org/10.1007/s00542-006-0194-z.
[41] D. Almonti, G. Baiocco, E. Menna, E. Mingione, G. Rubino, N. Ucciardello, Characterisation of Cu-GnP composite coatings for friction control and wear resistance applications, Eng. Fail. Anal. 139 (2022) 106419, https://doi.org/10.1016/j.engfailanal.2022.106419.
[42] M.A.M. Ibrahim, R.M. Al Radadi, Noncrystalline cobalt coatings on copper substrates by electrodeposition from complexing acidic glycine baths, Mater. Chem. Phys. 151 (2015) 222–232, https://doi.org/10.1016/j.matchemphys.2014.11.058.
[43] M.M. Abou-Krisha, Influence of $Ni2+$ concentration and deposition potential on the characterization of thin electrodeposited Zn–Ni–Co coatings, Mater. Chem. Phys. 125 (2011) 621–627, https://doi.org/10.1016/j.matchemphys.2010.10.007.
[44] A. Jabbar, G. Yasin, W.Q. Khan, M.Y. Anwar, R.M. Korai, M.N. Nizam, G. Muhyodin, Electrochemical deposition of nickel graphene composite coatings: effect of deposition temperature on its surface morphology and corrosion resistance, RSC Adv. 7 (2017) 31100–31109, https://doi.org/10.1039/C6RA28755G.
[45] J. Li, Z. An, Z. Wang, M. Toda, T. Ono, Pulse-reverse electrodeposition and micromachining of graphene-nickel composite: an efficient strategy toward high-performance microsystem application, ACS Appl. Mater. Interfaces 8 (2016) 3969–3976, https://doi.org/10.1021/acsami.5b11164.
[46] E.S. Gadelmawla, M.M. Koura, T.M.A. Maksoud, I.M. Elewa, H.H. Soliman, Roughness parameters, J. Mater. Process. Technol. 123 (1) (2002) 133–145.
[47] S. Qi, X. Li, H. Dong, Reduced friction and wear of electro-brush plated nickel composite coatings reinforced by graphene oxide, Wear 426–427 (2019) 228–238.
[48] H. Algul, M. Tokur, S. Ozcan, M. Uysal, T. Cetinkaya, H. Akbulut, A. Alp, The effect of graphene content and sliding speed on the wearmechanism of nickel–graphene nanocomposites, App. Surf. Sci. 359 (2015) 340–348.
[49] Y. Wana, L. Chen, W. Tangc, J. Li, Effect of graphene on tribological properties of Ni based composite coatings prepared by oxidation reduction method, J. Mater. Technol. 9 (3) (2020) 3796–3804.
[50] X. Li, Q. Shen, Y. Zhang, L. Wang, C. Nie, Wear behavior of electrodeposited nickel/graphene composite coating, Diam. Relat. Mater. 119 (2021) 108589, https://doi.org/10.1016/j.diamond.2021.108589.
[51] Y. Liu, F. Zheng, Y. Wu, C.C. Koch, P. Han, C. Zhang, Y. Liu, Y. Zhang, Grain refinement induced friction reduction and anti-wear performances of electrodeposited graphene/Ni composites with low content reduced graphene oxide, J. Alloy. Compd. 826 (2020) 154080, https://doi.org/10.1016/j.jallcom.2020.154080.
[52] D. Zhang, X. Cui, G. Jin, D. Li, Y. Fang, X. Wen, G. Ma, H. Wang, B. Xu, Comparison of MWCNTs and GO reinforced electro-brush plated ni nanocomposite coatings: structural variations of carbon-based reinforcements and tribological behavior, J. Alloy. Compd. 832 (2020) 154941, https://doi.org/10.1016/j.jallcom.2020.154941.
[53] J. Chen, J. Li, X. Xiong, Y. He, Y. Ji, Y. Qin, Preparation and tribological behavior of Ni-graphene compositecoating under room temperature, App. Surf. Sci. 361 (2016) 49–56, https://doi.org/10.1016/j.apsusc.2015.11.094.